

PROTOADA: Prototype-Guided Adaptive Adapter Expansion and Geometric Consolidation for Multimodal Continual Instruction Tuning

Yu-Cheng Shi^{*2}, Zhen-Hao Xie^{*1,2}, Jun-Tao Tang², Da-Wei Zhou^{1,2,†}

¹ School of Artificial Intelligence, Nanjing University, China

² State Key Laboratory of Novel Software Technology, Nanjing University, China

^{*} Equal contribution [†] Corresponding Author

{231250034, juntao.tang}@smail.nju.edu.cn, {wenzh, zhoudw}@lamda.nju.edu.cn

Abstract

Multimodal Large Language Models (MLLMs) achieve strong performance through instruction tuning, but real-world deployment requires them to continually acquire new vision-language capabilities, making Multimodal Continual Instruction Tuning (MCIT) essential. To reduce inter-task interference and promote collaboration, recent methods often employ sparse architectures like Mixture of LoRA Experts with image-text similarity routing. However, tasks with distinct response structures could share highly similar visual-linguistic semantics and thus be wrongly routed to the same expert; image-text similarity alone is insufficient for reliable task assignment. For example, an expert in a grounding task requiring coordinate prediction may be biased toward producing short textual answers after learning semantically similar VQA tasks. This format-blind task assignment integrates heterogeneous response types into shared parameters, inducing gradient interference and ineffective expert collaboration. To address this problem, we propose PROTOADA, a prototype-guided adaptive tuning framework. PROTOADA introduces format-aware task prototypes to align task assignment and routing with both task semantics and output structure, and further consolidates format-compatible updates in a geometry-aware manner to effectively reuse and progressively refine existing parameters. Extensive experiments on multiple benchmarks demonstrate that PROTOADA achieves superior performance, especially on tasks whose answer structures are easily corrupted by sequential tuning.

1 Introduction

Recently, multimodal Large Language Models (MLLMs) (Bai et al., 2023; Liu et al., 2023; Zhu et al., 2023) have shown strong generalization through multimodal instruction tuning (Zhang et al., 2023a; Tong et al., 2025) on large-scale datasets, enabling a wide range of vision-language

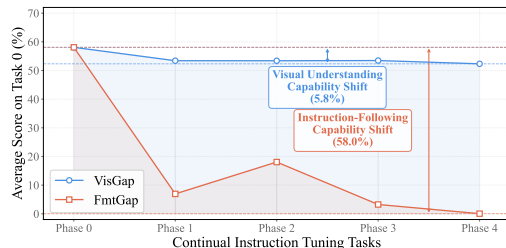


Figure 1: Accuracy of sequential finetuning under format-varied (FmtGap) and semantic-varied (VisGap) continual tuning streams.

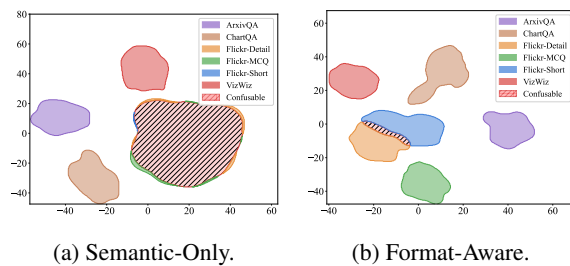


Figure 2: t-SNE visualization of task representations under semantic-only and format-aware prototypes.

tasks (Radford et al., 2021; Dai et al., 2023; Guo et al., 2025c). In realistic scenarios, however, multimodal tasks (Hu and Singh, 2021; Yang et al., 2025) often arrive sequentially, requiring multimodal continual instruction tuning (MCIT) (Chen et al., 2024) to continually acquire new capabilities after deployment, without access to previous training data. This setting is challenging due to catastrophic forgetting (French, 1999; French and Ferrara, 2020), where learning new tasks may overwrite not only previously learned semantic knowledge but also task-specific output conventions (Liu et al., 2025b). Recent works introduce parameter-efficient adaptation to improve the stability-plasticity trade-off (Zeng et al., 2025; Yu et al., 2025; Zhao et al., 2025; Huai et al., 2025; Wang et al., 2025b), with MoE-style parameter isolation mitigating interference by routing tasks

to sparsely activated lightweight experts, typically based on image-text semantic similarity. However, semantic similarity alone cannot determine whether tasks should share the same adaptation path: tasks involving similar visual regions and instructions may require incompatible output protocols, such as bounding-box coordinates versus short textual phrases. Such mismatches can entangle heterogeneous formats within experts, motivating an explicit format-aware mechanism for MCIT.

Format-induced incompatibility suggests that the failure of semantic routing may arise from a deeper mismatch: semantically similar instructions can require fundamentally different response protocols. To verify this, we construct two controlled continual-learning streams under the same parameter-sharing setup. The first keeps the visual-semantic content fixed by using Flickr30k (Plummer et al., 2015), but varies the response protocol across five formats¹; the second keeps the output format as brief description, but mixes different datasets like Flickr30k and VizWiz (Gurari et al., 2018) to introduce visual-semantic shifts. As shown in Fig. 1, sequential tuning degrades performance in both streams, but the decline is substantially larger under format variation. This result indicates that MLLM tuning not only learns visual-linguistic associations but also aligns instructions with expected answer forms. Therefore, visual-linguistic similarity is insufficient for parameter-sharing decisions, and response-protocol compatibility should be explicitly considered.

This raises a practical question: can response formats be captured in a lightweight way before deciding task sharing? For each task, we construct two representations from frozen image-text embeddings: a semantic-only prototype and a format-aware prototype augmented with simple response statistics, such as average length and token entropy. The t-SNE (Van der Maaten and Hinton, 2008) visualization in Fig. 2 shows that semantic-only embeddings poorly separate tasks with different answer protocols, while the lightweight format code makes these protocols more distinguishable. This suggests that response statistics can serve as an effective proxy for instruction-following patterns, guiding task grouping to encourage sharing among compatible protocols while reducing interference between incompatible ones.

¹The five formats are brief description, detailed description, short/one-word answer, multiple choice answer, and yes/no answer.

These observations suggest that effective MCIT should both identify incompatible response protocols to avoid format-specific conflicts and consolidate compatible updates for parameter reuse. To this end, we propose PROTOADA, a prototype-guided adaptive tuning framework that builds format-aware task prototypes from visual, language, and response-format statistics, grouping tasks by both content and expected answer protocol. Within each group, PROTOADA performs geometry-aware consolidation: group-aligned directions refine shared parameters, while residual directions are preserved to protect task-specific response conventions. Experiments on multiple benchmarks demonstrate the effectiveness of PROTOADA on complex continual data streams.

2 Related Work

As MLLMs are increasingly deployed in open-world scenarios, continual instruction tuning (Chen et al., 2024; Liu et al., 2025b) becomes essential for acquiring new capabilities without overwriting old ones. Existing methods mainly follow three directions. Replay-based methods (Li et al., 2025; Yu et al., 2025) retain or synthesize previous image-text samples to stabilize later training, but the required storage and computation increase as the task stream grows (Lee et al., 2025). Regularization- and prompt-based methods (Wang et al., 2023; Cao et al., 2024; Liu et al., 2025a) constrain representation drift or introduce lightweight task-specific prompts, improving efficiency but often relying on semantic task similarity or task identity cues that can be unreliable when visually similar tasks require different answer formats (Zeng et al., 2025; Chen et al., 2025). Parameter-efficient and expert-based methods (Guo et al., 2025a; Zhao et al., 2025; Huai et al., 2025; Wang et al., 2025b) further introduce LoRA modules, adapter pools, or mixture-of-experts structures to isolate task-specific knowledge and reduce interference.

3 Preliminaries

3.1 Multimodal continual instruction tuning

We consider a multimodal large language model consisting of a frozen vision encoder ϕ , a multimodal projector π , and a large language model f equipped with lightweight trainable modules. Let $\{\mathcal{T}_1, \mathcal{T}_2, \dots, \mathcal{T}_N\}$ denote a sequence of multimodal instruction-tuning tasks, where each $\mathcal{T}_i = \{(v_j, q_j, y_j)\}_{j=1}^{M_i}$ contains an image v_j , an instruc-

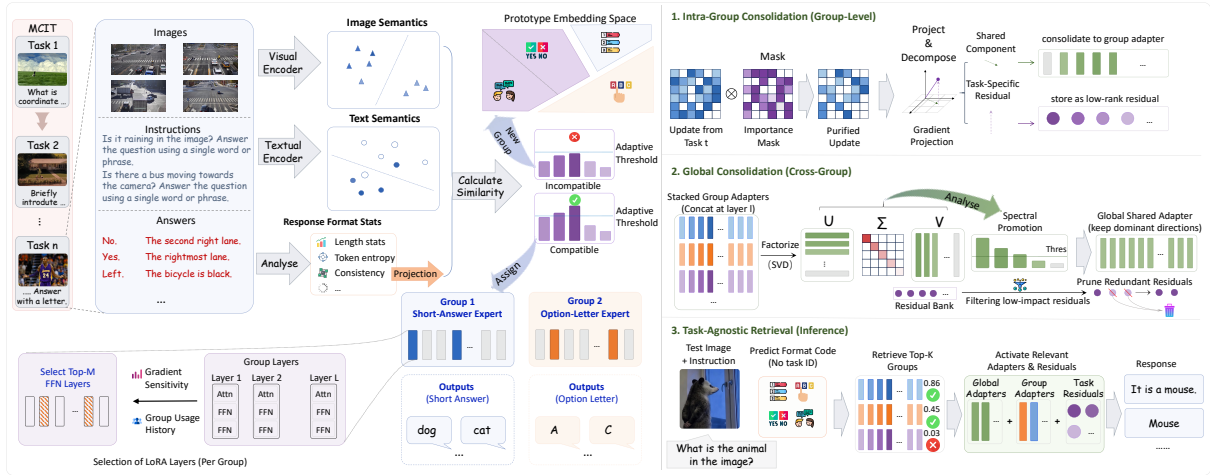


Figure 3: PROTOADA groups tasks with compatible response formats into shared experts, while separating conflicting formats and adapting only the most sensitive layers within each group.

tion q_j , and a target response $y_j = (y_{j,1}, \dots, y_{j,L_j})$. The frozen vision encoder extracts visual features $\tilde{\mathbf{v}} = \phi(v)$, the embedding layer $\psi(\cdot)$ produces instruction embeddings $\mathbf{u} = \psi(q)$, and the projector maps visual features into the language space as $\mathbf{w} = \pi(\tilde{\mathbf{v}})$, forming the multimodal input $\mathbf{z} = [\mathbf{w}; \mathbf{u}]$. Given a target response token sequence $y = (y_1, \dots, y_L)$, the MLLM models the conditional distribution:

$$p_{\Theta}(y | z) = \prod_{k=1}^{L_j} p_{\Theta}(y_k | \mathbf{z}, y_{<k}). \quad (1)$$

The goal of MCIT is to obtain a unified model that performs well on all tasks observed so far. After step i , the ideal objective is

$$\Theta_i^* = \arg \min_{\Theta} \mathbb{E}_{(v,q,y) \sim \mathcal{T}_{<i}} [-\log p_{\Theta}(y | \mathbf{z})], \quad (2)$$

where $\mathcal{T}_{<i}$ denotes the union of all seen task distributions. In rehearsal-free MCIT, however, optimization at step i only accesses \mathcal{T}_i , and thus the learner must improve the current task likelihood while preserving behaviors induced by previous tasks without revisiting their samples. This mismatch of data distribution is the fundamental source of forgetting.

3.2 Low-rank adaptation in the language model

We adopt a rehearsal-free parameter-efficient setting in which the vision encoder, projector, and pretrained language backbone are frozen, and trainable parameters are introduced only through LoRA

modules inserted into all linear modules of the language model. For a linear module ℓ with frozen weight W_{ℓ} , LoRA modifies its output as

$$\mathbf{o}_{\ell} = \mathbf{W}_{\ell} \mathbf{h}_{\ell} + \mathbf{B}_{\ell} \mathbf{A}_{\ell} \mathbf{h}_{\ell}, \quad (3)$$

where $\mathbf{A}_{\ell} \in \mathbb{R}^{r \times d_{\text{in}}}$ and $\mathbf{B}_{\ell} \in \mathbb{R}^{d_{\text{out}} \times r}$ are trainable low-rank factors with rank r . Only $\Theta = \{\mathbf{A}_{\ell}, \mathbf{B}_{\ell}\}_{\ell \in \mathcal{L}}$ are updated. After learning task t , we denote the LoRA increment as $\Delta \Theta_t = \Theta_t - \Theta_{t-1}$, which must adapt to the current task while avoiding disruption to previously learned instruction-following behaviors. LoRA-based continual instruction tuning thus requires careful decisions about which parameter group receives a new task and how its update is consolidated.

Discussions. The gap between the ideal objective in Eq. (2) and rehearsal-free training makes LoRA updates shown in Eq. (3) vulnerable to structural interference: when task allocation relies mainly on image-instruction semantics, tasks with similar inputs but incompatible answer formats may share the same LoRA group, corrupting the instruction-to-protocol mapping. This motivates PROTOADA, which represents tasks with visual, language, and format-aware prototypes before sharing parameters, and consolidates compatible updates to enable reliable reuse.

4 Method

To preserve instruction-following ability for MLLMs, we propose PROTOADA, a prototype-guided MCIT framework. PROTOADA organizes LoRA parameters into multiple memory groups,

where each group stores shared parameters for tasks that are compatible in both image-text semantics and response protocols. To avoid entangling incompatible instruction formats, when a new task arrives, PROTOADA builds a format-aware task prototype from visual semantics, language semantics, and response-format statistics. The task is then assigned to an existing group or a new group according to its compliance with old tasks inferred from its prototype. Compatible updates are then consolidated into the corresponding group, enabling parameter reuse while preserving task-specific output conventions.

4.1 Format-aware task grouping

To better represent tasks with prototypes and more effectively identify compatibility relations among tasks, given a task $\mathcal{T}_i = \{(v_{t,j}, q_{t,j}, y_{t,j})\}_{j=1}^{M_i}$, we first compute its language and visual descriptors using frozen visual and textual encoders such as CLIP (Radford et al., 2021):

$$\begin{aligned} \mathbf{p}_t^{\text{text}} &= \frac{1}{M_t} \sum_{j=1}^{M_t} E_{\text{text}}(q_{t,j}), \\ \mathbf{p}_t^{\text{vis}} &= \frac{1}{M_t} \sum_{j=1}^{M_t} E_{\text{vis}}(v_{t,j}). \end{aligned} \quad (4)$$

However, these descriptors only capture what the task is about, but not how the model should answer. As shown in Fig. 1, tasks with similar image-text semantics may require different response protocols. Routing such tasks only by image-text similarity can therefore force incompatible instruction formats into the same parameters and damage the model’s instruction-following behavior. To incorporate response protocols into task grouping, we calculate the mean, variance of response length, token uncertainty, and template consistency² from target responses and derive a format code:

$$\mathbf{c}_t^{\text{fmt}} = [\mu_\ell, \sigma_\ell, H_{\text{tok}}, C_{\text{fmt}}], \quad (5)$$

This format code is mapped into the prototype space by:

$$\mathbf{p}_t^{\text{fmt}} = \mathbf{W}_{\text{fmt}} \mathbf{c}_t^{\text{fmt}} + \mathbf{b}_{\text{fmt}}. \quad (6)$$

The final task prototype combines language, vision, and format information:

$$\mathbf{q}_t = \text{Norm} \left(\mathbf{W}_q [\mathbf{p}_t^{\text{text}} \parallel \mathbf{p}_t^{\text{vis}} \parallel \mathbf{p}_t^{\text{fmt}}] \right). \quad (7)$$

²Implementation details about the calculation of these format statistics are shown in Appendix C

Based on the format-aware task prototype, each memory group g is represented by a group prototype p_g that summarizes its assigned tasks. When a new task arrives, we compare its prototype q_t with all existing group prototypes to decide whether it can share an existing group or should initialize a new one:

$$s_{t,g} = \frac{\langle \mathbf{q}_t, \mathbf{p}_g \rangle}{\|\mathbf{q}_t\|_2 \|\mathbf{p}_g\|_2}, \quad g_t = \arg \max_g s_{t,g}. \quad (8)$$

Since different groups may exhibit different degrees of internal diversity, we adopt a dynamic admission threshold. Specifically, for each group g , we maintain the running mean μ_g and standard deviation σ_g of the similarities between previously assigned tasks and the group prototype \mathbf{p}_g . The assignment rule is then defined as:

$$\text{Assign}(t) = \begin{cases} g_t, & s_{t,g_t} \geq \mu_{g_t} - \sigma_{g_t}, \\ \text{new}, & s_{t,g_t} < \mu_{g_t} - \sigma_{g_t}. \end{cases} \quad (9)$$

If the task is assigned to an existing group, its prototype is updated as:

$$\mathbf{p}_{g_t} \leftarrow \text{Norm}((1 - \alpha)\mathbf{p}_{g_t} + \alpha\mathbf{q}_t). \quad (10)$$

Otherwise, a new group is initialized with \mathbf{q}_t . This allows compatible tasks to share LoRA parameters while separating tasks with conflicting response protocols. However, since the format is unavailable during inference, we therefore train a lightweight predictor f_{fmt} to infer it from input-side descriptors during training:

$$\hat{\mathbf{c}}_t^{\text{fmt}} = f_{\text{fmt}}(\mathbf{p}_t^{\text{text}}). \quad (11)$$

During inference, we replace \mathbf{c}^{fmt} with the predicted format code $\hat{\mathbf{c}}^{\text{fmt}}$ when constructing the task prototype, thereby enabling format-aware grouping under task-agnostic retrieval.

Discussions. By incorporating response protocols into task identity, Eq. (7) fuses visual, linguistic, and format cues, while Eq. (9) admits a task into a group only when it is compatible with the group’s historical prototype. The format predictor further extends this principle to task-agnostic inference, where target responses are unavailable.

4.2 Prototype-conditioned adaptive growth

Once a task has been assigned to a memory group, PROTOADA further decides what additional parameters should be introduced and where they should be placed. Adding Lora Modules to all layers for

every task is parameter-inefficient and may perturb stable behaviors, so we selectively adapt only the layers where the current task demands the most change. For each FFN layer ℓ , we estimate task sensitivity by the gradient energy of the task loss with respect to the hidden state:

$$\gamma_\ell = \mathbb{E}_{(v,q,y) \sim \mathcal{T}_i} \left[\left\| \frac{\partial \mathcal{L}_{ce}}{\partial \hat{h}_\ell} \right\|_2 \right]. \quad (12)$$

A larger γ_ℓ indicates that layer ℓ is more involved in fitting the current task and is therefore a better candidate for adaptation.

To avoid repeatedly allocating capacity to only a few high-gradient layers, we further incorporate the historical layer-usage pattern of the assigned memory group. Since tasks in the same group share compatible instruction-following behaviors, adapting a historically used layer is more likely to reuse an established adaptation path rather than open an unrelated one. We thus combine current-task sensitivity with group-level usage:

$$\begin{aligned} \tilde{\gamma}_\ell &= \gamma_\ell + \eta u_{g_t, \ell}, \\ \mathcal{S}_t &= \text{TopM}(\{\tilde{\gamma}_\ell\}_{\ell=1}^L; M), \end{aligned} \quad (13)$$

where $u_{g_t, \ell}$ records how frequently group g_t has used layer ℓ , and \mathcal{S}_t is the set of Linear layers selected for adaptation. Only the modules in \mathcal{S}_t are updated for the current task.

Discussions. This mechanism refines the memory assignment made by the prototype: the prototype decides which group hosts the task, while the sensitivity-and-usage score decides where new capacity is introduced within that group. The usage term provides a soft reuse prior for compatible tasks, while the sensitivity term still allows new layers to be selected when the current task demands them, balancing parameter reuse and task-specific expansion under format-aware grouping.

4.3 Geometry-aware consolidation and task-agnostic retrieval

After task t is assigned to group g_t and optimized, the LoRA increment $\Delta\Theta_t$ contains two types of information: group-compatible knowledge that benefits future tasks in the same group, and task-specific corrections that only preserve the current task’s response behavior. Merging the whole update into the group adapter would entangle these two components and let fragile response protocols interfere with shared abilities. We therefore decouple the

reusable part of each update from its task-specific residual before consolidation.

Since not every changed parameter is equally supported by the current task, we first compute an activation-aware importance score:

$$I_t(i, j) = |\Delta\Theta_t(i, j)| a_j, \quad (14)$$

where $a_j = \|\mathbf{X}_{:,j}\|_2$ is the input activation norm of channel j . Keeping the top- $k\%$ entries yields a purified update (Sun et al., 2024):

$$\Delta\hat{\Theta}_t = \mathbf{M}_t \odot \Delta\Theta_t, \quad (15)$$

which is then decomposed according to the geometry of the assigned group. Let \mathcal{U}_{g_t} denote the subspace spanned by the current shared memory of group g_t , and let $\text{Proj}_{\mathcal{U}_{g_t}}(\cdot)$ be the orthogonal projection onto this subspace. The component aligned with the group memory is absorbed into the shared adapter, while the orthogonal component is kept as a compact task-specific residual:

$$\begin{aligned} \Delta\Theta_t^{\text{share}} &= \text{Proj}_{\mathcal{U}_{g_t}}(\Delta\hat{\Theta}_t), \\ \Delta\Theta_t^{\text{res}} &= \Delta\hat{\Theta}_t - \Delta\Theta_t^{\text{share}}. \end{aligned} \quad (16)$$

Here, $\Delta\Theta_t^{\text{share}}$ captures directions reusable by the assigned group, whereas $\Delta\Theta_t^{\text{res}}$ preserves task-specific deviations outside the group subspace.

The shared component updates the memory of the assigned group with a prototype-dependent weight. Let \mathbf{A}_g denote the shared adapter parameters maintained by group g . We update the selected group as:

$$\begin{aligned} \mathbf{A}_{g_t} &\leftarrow \mathbf{A}_{g_t} + \lambda_{t,g_t} \Delta\Theta_t^{\text{share}}, \\ \lambda_{t,g} &= \lambda_0 \frac{\exp(\beta s_{t,g})}{\sum_{g'} \exp(\beta s_{t,g'})}. \end{aligned} \quad (17)$$

So tasks closer to the group prototype contribute more strongly. The residual is compressed by truncated singular value decomposition (Klema and Laub, 1980) as:

$$\mathbf{R}_t = \text{SVD}_{r_{\text{res}}}(\Delta\Theta_t^{\text{res}}), \quad (18)$$

which preserves task-specific corrections without storing a dense task copy. To avoid redundant memory growth, we periodically reorganize the memory hierarchy. After every K newly observed tasks, the group adapters at layer ℓ are concatenated as

$$W_{\text{all}, \ell} = [\mathbf{A}_{\ell,1} \|\mathbf{A}_{\ell,2}\| \cdots \|\mathbf{A}_{\ell,G}], \quad (19)$$

and their dominant spectral directions are promoted into a global shared adapter:

$$\mathbf{A}_\ell^{\text{shared}} \leftarrow \mathbf{A}_\ell^{\text{shared}} + \Delta \mathbf{A}_\ell^{\text{global}}. \quad (20)$$

Residuals already explained by shared or group memory are then removed from the residual bank according to their coverage ratio

$$\rho_t = \frac{\left\| \text{Proj}_{\mathcal{U}_{\text{shared}} \cup \mathcal{U}_{g_t}}(\mathbf{R}_t) \right\|_F}{\left\| \mathbf{R}_t \right\|_F}. \quad (21)$$

During inference, since the task identity is unavailable, we construct a query prototype using the predicted format code and retrieve the top compatible groups with similarity-based weights

$$w_g = \frac{\exp(s_g/\tau)}{\sum_{g' \in \text{TopK}} \exp(s_{g'}/\tau)}, \quad (22)$$

and activates only residuals whose stored prototypes are close to the query. The prediction is produced by augmenting the frozen backbone with the global adapter, the retrieved group-level adapters, and the selected task residuals. This enables task-specific knowledge to be organized and retrieved within a unified format-aware prototype space.

4.4 Summary of PROTOADA

Overall, PROTOADA runs as a unified MCIT pipeline based on a set of memory groups. For each incoming task, we first build a format-aware prototype from frozen visual and textual descriptors together with a format code (Eqs. (4)–(7)), which is extracted from target responses during training and predicted by a lightweight predictor at inference (Eq. (11)). The prototype is then compared with existing group prototypes (Eqs. (8)–(10)), so that the task either joins a compatible group or seeds a new one. Within the assigned group, LoRA modules are inserted only at layers that are both sensitive to the current task and historically used by the group (Eqs. (12)–(13)), and are optimized by a cross-entropy loss together with an MSE loss for the format predictor, while the backbone and prior adapters stay frozen. The resulting update is then purified by activation-aware masking and split into a group-compatible component and an orthogonal residual (Eqs. (14)–(16)); the former is absorbed into the group adapter, and the latter is compressed via truncated SVD (Eqs. (17)–(18)). Periodic spectral promotion further extracts common directions into the global adapter and prunes

redundant residuals (Eqs. (19)–(21)). At inference, the predicted format code yields a query prototype that retrieves the most compatible groups and residuals (Eq. (22)), and the frozen backbone augmented with the global, group, and selected residual adapters produces the response in a single forward pass, all within one shared format-aware prototype space.

5 Experiments

5.1 Experimental Setup

Benchmarks. We evaluate PROTOADA on the following two benchmarks: TriGap (Xie et al., 2026) introduces challenges through longer task sequences, broader domain shifts, and imbalanced data scales, encompassing ten tasks: PMCVA (Zhang et al., 2023b), DocVQA (Mathew et al., 2021), ChartQA (Masry et al., 2022), IconQA (Lu et al., 2021), InfographicVQA (Mathew et al., 2022), ArxivQA (Li et al., 2024), Roadside (Guan et al., 2026), ChemVQA (Sabando et al., 2020), FloodNetVQA (Rahnemoonfar et al., 2021), and CLEVR-Math (Lindström and Abraham, 2022). UCIT (Guo et al., 2025a) employs strict filtering to mitigate pre-training contamination and comprises six tasks: ArxivQA (Li et al., 2024), CLEVR-Math (Lindström and Abraham, 2022), IconQA (Lu et al., 2021), ImageNet-R (Hendrycks et al., 2021), VizWiz-Caption (Gurari et al., 2018), and Flickr30k (Plummer et al., 2015).

Evaluation metrics. Following Zhou et al. (2024); Chen et al. (2024), we denote by $\mathcal{A}_{s,t}$, the performance on task s evaluated after training up to task t , with T total tasks. We summarize the average final performance by $\bar{\mathcal{A}} = \frac{1}{T} \sum_{s=1}^T \mathcal{A}_{s,T}$.

Compared Methods. We compare PROTOADA with state-of-the-art MCIT methods, including zero-shot evaluation (Liu et al., 2023), standard FineTune (Hu et al., 2022), MoELoRA (Chen et al., 2024), Replay-LoRA, HiDe-LLaVA (Guo et al., 2025a), CL-MoE (Huai et al., 2025), Modal-Prompt (Zeng et al., 2025), DISCO (Guo et al., 2025b), and SAME (Xie et al., 2026). Zero-shot results serve as a lower-bound reference. To ensure a fair comparison, all methods use identical backbone architectures and data protocols.

Implementation details. All experiments are conducted on 4 NVIDIA RTX 5090 GPUs. We follow Prism (Tang et al., 2026) to conduct all experiments. Following Chen et al. (2024); Xie et al. (2026), we

Table 1: Performance on TriGap. The best and second-best results are highlighted in **bold** and underline, respectively.

Methods	PMCVQA	DocVQA	ChartQA	IconQA	InfographicVQA	ArxivQA	Roadside	ChemVQA	FloodNetVQA	CLEVR	Average
Zero-shot (Liu et al., 2023)	35.40	12.68	9.36	19.27	5.06	53.77	7.40	5.30	47.41	20.37	21.60
FT-LoRA (Hu et al., 2022)	34.20	23.32	9.84	37.07	23.53	83.83	7.00	12.70	80.31	60.27	37.21
Replay-LoRA	33.70	33.95	14.00	46.67	28.97	75.57	9.40	15.90	73.81	58.80	39.08
MoE-LoRA (Chen et al., 2024)	39.03	37.49	12.44	43.43	35.17	90.90	7.93	20.70	90.41	67.00	44.45
HiDe-LLaVA (Guo et al., 2025a)	37.00	33.20	10.52	41.97	24.09	79.20	7.73	11.17	57.39	23.00	32.53
ModalPrompt (Zeng et al., 2025)	38.23	38.23	11.92	44.73	37.37	84.47	10.13	12.43	71.52	52.50	40.15
CL-MoE (Huai et al., 2025)	40.53	36.79	13.72	52.70	32.27	<u>93.00</u>	7.77	18.33	80.09	<u>65.90</u>	44.11
SAME (Xie et al., 2026)	41.60	43.87	17.56	<u>64.03</u>	39.57	90.46	<u>10.83</u>	21.77	<u>81.09</u>	54.50	46.53
DISCO (Guo et al., 2025b)	<u>42.03</u>	<u>43.50</u>	<u>18.01</u>	63.13	<u>38.23</u>	91.27	<u>11.02</u>	<u>22.13</u>	80.25	55.87	<u>46.54</u>
PROTOADA (Ours)	42.87	43.01	18.96	66.03	36.31	93.50	12.97	23.73	74.03	57.87	47.23

Table 2: Average performance of different methods on the UCIT benchmark. The best and second-best results are highlighted in **bold** and underline, respectively.

Methods	ImageNet-R	ArxivQA	Vizcap	IconQA	CLEVER	Flickr30k	Average
Zero-shot (Liu et al., 2023)	18.88	52.62	38.75	21.25	21.12	41.44	32.34
FT-LoRA (Hu et al., 2022)	29.33	55.30	45.51	26.13	13.07	<u>58.07</u>	37.90
MoE-LoRA (Chen et al., 2024)	58.43	77.57	44.83	68.90	56.73	58.27	60.79
Replay-LoRA	76.93	87.07	54.31	56.43	36.40	55.94	61.18
CL-MoE (Huai et al., 2025)	64.12	78.38	44.83	62.00	50.75	58.06	59.69
HiDe-LLaVA (Guo et al., 2025a)	87.62	91.12	42.68	57.62	31.00	50.41	60.08
ModalPrompt (Zeng et al., 2025)	80.50	90.62	<u>60.13</u>	63.50	55.75	57.09	67.93
DISCO (Guo et al., 2025b)	88.88	94.25	47.52	69.50	60.75	56.32	69.54
SAME (Xie et al., 2026)	89.91	91.40	55.33	<u>77.51</u>	68.85	55.43	<u>73.07</u>
PROTOADA (Ours)	<u>89.83</u>	<u>93.20</u>	61.49	81.37	<u>66.40</u>	55.64	74.66

use LLaVA-v1.5-7B (Liu et al., 2023) as the backbone MLLM and CLIP-L/14-336 (Radford et al., 2021) to extract visual and textual features. The vision encoder, projector, and pretrained language model are frozen, and trainable low-rank modules are inserted into all linear layers of the language model (Wang et al., 2025a; Zhu et al., 2025). Each task is trained for 1 epoch using the AdamW optimizer with a learning rate of $2e - 4$ and a linear warm-up ratio of 0.03. Unless otherwise specified, the initial rank is set to $r_0 = 8$ for each task in TriGap and $r_0 = 16$ for each task in UCIT. For PROTOADA, the residual rank is $r_{\text{res}} = 2$, the number of selected FFN layers is $M = 24$, and spectral memory maintenance is performed every $K = 5$ tasks. The format predictor is a two-layer MLP trained jointly with the task loss.

5.2 Benchmark Comparison and Ablation

Benchmark Comparison. We compare PROTOADA with representative continual instruction tuning baselines on TriGap and UCIT, as reported in Tab. 1 and Tab. 2. On the more challenging TriGap benchmark, PROTOADA achieves the best average accuracy of 47.23%, showing its robustness under longer task sequences and more heterogeneous response protocols. Consistent gains on UCIT further validate the effectiveness of our format-aware and consolidation-aware design, which enables compatible LoRA sharing while preserving task-specific instruction-following behav-

Table 3: Ablation study of PROTOADA, all experiments are conducted under UCIT.

Variant	Avg. Acc (%)
Baseline	60.79
w/ Format	68.13
w/ Format + Adaptive	72.35
w/ Format + Adaptive + Geometry (Ours)	74.66

iors across benchmarks.

Ablation Study. Tab. 3 studies the contribution of each component in our method. We use MoELoRA as the baseline and fix the LoRA rank to 8 for all variants. Format-aware prototypes improve the average accuracy from 60.79% to 68.13% by grouping tasks with compatible response formats. Adaptive assignment further increases accuracy to 72.35% through more flexible memory selection. Method with Geometry-aware consolidation (full PROTOADA) achieves the best result of 74.66% by preserving task-specific update residuals while sharing common directions.

5.3 Further Analysis

Stress Test on Controlled Format Streams. To verify whether PROTOADA addresses the failure mode identified in Fig. 1, we replay the two controlled streams from the preliminary study and compare full continual learners. As shown in Fig. 4, all methods achieve similar Last accuracy on the same-format stream, mostly around 52–55%, indicating that the response protocol itself does not

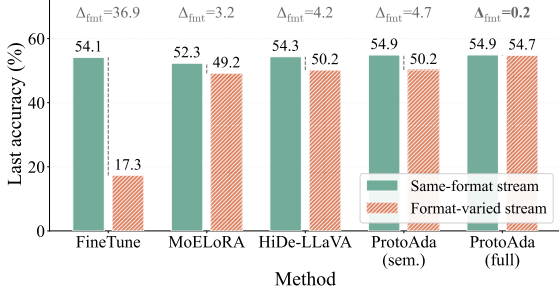


Figure 4: Performance gap between handling streams with the same format and streams with varied formats.

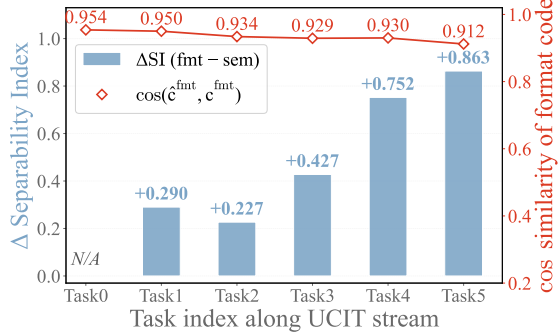


Figure 5: Separability index among task prototypes on UCIT as more tasks are learned, with the line tracking similarity between predicted and oracle format codes.

cause severe degradation when it remains consistent. In contrast, the format-varied stream leads to a large drop for FineTune, whose Last accuracy decreases from 54.1% to 17.3% with $\Delta_{fmt} = 36.9$. MoELoRA, HiDe-LLaVA, and the semantic-only variant of PROTOADA reduce this gap but still suffer clear format-induced forgetting, with Δ_{fmt} ranging from 3.2 to 4.7. Once format-aware prototypes are enabled, the gap is almost eliminated, with PROTOADA reaching 54.7% on the format-varied stream and reducing Δ_{fmt} to only 0.2. This shows that the observed format mismatch is not only diagnostic but can be effectively mitigated by conditioning task allocation on response protocols.

Temporal Dynamics of Format-Aware Prototypes. The visualization in Fig. 2 shows that a lightweight format code separates tasks with different response protocols at a single snapshot, and a natural follow-up question is whether this structure remains stable while new tasks are continuously inserted. Fig. 5 tracks this effect along the UCIT stream. Compared with semantic-only prototypes, format-aware prototypes consistently improve the separability index, with ΔSI increasing from +0.290 at Task1 to +0.863 at Task5. Meanwhile, the predicted format code \hat{c}^{fmt} remains

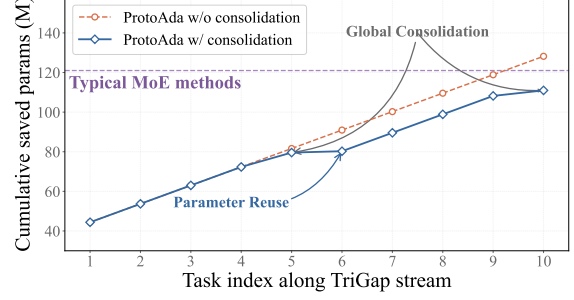


Figure 6: Parameter budget of PROTOADA over the Tri-Gap task stream.

highly aligned with the oracle c^{fmt} , with cosine similarity staying above 0.91 throughout the stream. These results indicate that the format prototype is not only a useful one-shot descriptor as suggested in Fig. 2, but also a stable basis for continual task assignment and task-agnostic retrieval.

Parameter Growth under Selective Expansion and Consolidation.

A core claim of PROTOADA is that selective layer expansion in Eq. (13) and spectral consolidation in Eq. (20) keep memory growth controlled rather than letting parameters accumulate linearly. Fig. 6 records the cumulative saved adapter parameters along the TriGap task stream. Without consolidation, the parameter count grows steadily and reaches about 128M at Task10, exceeding the typical MoE budget after Task9. In contrast, PROTOADA with consolidation grows more slowly after reuse begins around Task5 and remains below the MoE budget, ending at about 111M. The widening gap in later tasks shows that global consolidation promotes reusable directions instead of storing every task update independently. Together with the previous analyses, this confirms that PROTOADA improves continual adaptation by reusing compatible directions while preserving task-specific residuals.

6 Conclusion

We identify format-blind task assignment as a key source of forgetting in MCIT and propose PROTOADA, which performs format-aware task grouping, selective LoRA expansion, and geometry-aware update consolidation. By reusing compatible knowledge while preserving task-specific response conventions, PROTOADA achieves stronger continual adaptation across multiple benchmarks.

Limitations

Although PROTOADA achieves strong performance on current MCIT benchmarks, its effectiveness has not yet been validated on substantially longer task streams or more diverse response protocols beyond the evaluated settings. Extending PROTOADA to larger-scale continual streams and more open-ended multimodal instruction scenarios remains an important direction for future work.

References

- Jinze Bai, Shuai Bai, Shusheng Yang, Shijie Wang, Sinan Tan, Peng Wang, Junyang Lin, Chang Zhou, and Jingren Zhou. 2023. Qwen-vl: A versatile vision-language model for understanding, localization, text reading, and beyond. *arXiv preprint arXiv:2308.12966*.
- Meng Cao, Yuyang Liu, Yingfei Liu, Tiancai Wang, Jiahua Dong, Henghui Ding, Xiangyu Zhang, Ian Reid, and Xiaodan Liang. 2024. Continual llava: Continual instruction tuning in large vision-language models. *arXiv preprint arXiv:2411.02564*.
- Cheng Chen, Junchen Zhu, Xu Luo, Heng T Shen, Jingkuan Song, and Lianli Gao. 2024. Coin: A benchmark of continual instruction tuning for multimodal large language models. *Advances in Neural Information Processing Systems*, pages 57817–57840.
- Jinpeng Chen, Runmin Cong, Yuzhi Zhao, Hongzheng Yang, Guangneng Hu, Horace Ip, and Sam Kwong. 2025. SEFE: Superficial and essential forgetting eliminator for multimodal continual instruction tuning. In *International Conference on Machine Learning*, pages 7982–8001.
- Wenliang Dai, Junnan Li, Dongxu Li, Anthony Tiong, Junqi Zhao, Weisheng Wang, Boyang Li, Pascale N Fung, and Steven Hoi. 2023. Instructblip: Towards general-purpose vision-language models with instruction tuning. *Advances in Neural Information Processing Systems*, 36:49250–49267.
- Robert M French. 1999. Catastrophic forgetting in connectionist networks. *Trends in cognitive sciences*, 3(4):128–135.
- Robert M French and André Ferrara. 2020. Modeling time perception in rats: Evidence for catastrophic interference in animal learning. In *Proceedings of the Annual Conference of the Cognitive Science Society*, pages 173–178. Psychology Press.
- Runwei Guan, Rongsheng Hu, Shangshu Chen, Ningyuan Xiao, Xue Xia, Jiayang Liu, Beibei Chen, Ziren Tang, Ningwei Ouyang, Shaofeng Liang, and 1 others. 2026. Roadscenevqa: Benchmarking visual question answering in roadside perception systems for intelligent transportation system. In *Proceedings of the AAAI Conference on Artificial Intelligence*, pages 4366–4375.
- Haiyang Guo, Fanhu Zeng, Ziwei Xiang, Fei Zhu, Da-Han Wang, Xu-Yao Zhang, and Cheng-Lin Liu. 2025a. Hide-llava: Hierarchical decoupling for continual instruction tuning of multimodal large language model. In *Proceedings of the Annual Meeting of the Association for Computational Linguistics*, pages 13572–13586.
- Haiyang Guo, Fanhu Zeng, Fei Zhu, Wenzhuo Liu, Da-Han Wang, Jian Xu, Xu-Yao Zhang, and Cheng-Lin Liu. 2025b. Federated continual instruction tuning. In *Proceedings of the IEEE international conference on computer vision*, pages 1325–1335.
- Jiawei Guo, Tianyu Zheng, Yizhi Li, Yuelin Bai, Bo Li, Yubo Wang, King Zhu, Graham Neubig, Wenhua Chen, and Xiang Yue. 2025c. Mammoth-vl: Eliciting multimodal reasoning with instruction tuning at scale. In *Proceedings of the Annual Meeting of the Association for Computational Linguistics*, pages 13869–13920.
- Danna Gurari, Qing Li, Abigale J Stangl, Anhong Guo, Chi Lin, Kristen Grauman, Jiebo Luo, and Jeffrey P Bigham. 2018. Vizwiz grand challenge: Answering visual questions from blind people. In *Proceedings of the IEEE/CVF Computer Vision and Pattern Recognition Conference*, pages 3608–3617.
- Dan Hendrycks, Steven Basart, Norman Mu, Saurav Kadavath, Frank Wang, Evan Dorundo, Rahul Desai, Tyler Zhu, Samyak Parajuli, Mike Guo, and 1 others. 2021. The many faces of robustness: A critical analysis of out-of-distribution generalization. In *Proceedings of the IEEE international conference on computer vision*, pages 8340–8349.
- Edward J Hu, Yelong Shen, Phillip Wallis, Zeyuan Allen-Zhu, Yuanzhi Li, Shean Wang, Lu Wang, Weizhu Chen, and 1 others. 2022. Lora: Low-rank adaptation of large language models. *International Conference on Learning Representations*.
- Ronghang Hu and Amanpreet Singh. 2021. Unit: Multimodal multitask learning with a unified transformer. In *Proceedings of the IEEE international conference on computer vision*, pages 1439–1449.
- Tianyu Huai, Jie Zhou, Xingjiao Wu, Qin Chen, Qingchun Bai, Ze Zhou, and Liang He. 2025. Clmoe: Enhancing multimodal large language model with dual momentum mixture-of-experts for continual visual question answering. In *Proceedings of the IEEE/CVF Computer Vision and Pattern Recognition Conference*, pages 19608–19617.
- Virginia Klema and Alan Laub. 1980. The singular value decomposition: Its computation and some applications. *IEEE Transactions on automatic control*, 25(2):164–176.
- Minjae Lee, Minhyuk Seo, Tingyu Qu, Tinne Tuytelaars, and Jonghyun Choi. 2025. Oasis: Online sample selection for continual visual instruction tuning. *arXiv preprint arXiv:2506.02011*.

- Lei Li, Yuqi Wang, Runxin Xu, Peiyi Wang, Xiachong Feng, Lingpeng Kong, and Qi Liu. 2024. Multimodal arxiv: A dataset for improving scientific comprehension of large vision-language models. In *Proceedings of the Annual Meeting of the Association for Computational Linguistics*, pages 14369–14387.
- Songze Li, Mingyu Gao, Tonghua Su, Xu-Yao Zhang, and Zhongjie Wang. 2025. Multimodal continual instruction tuning with dynamic gradient guidance. *arXiv preprint arXiv:2511.15164*.
- Adam Dahlgren Lindström and Savitha Sam Abraham. 2022. Clevr-math: A dataset for compositional language, visual and mathematical reasoning. *arXiv preprint arXiv:2208.05358*.
- Haotian Liu, Chunyuan Li, Qingyang Wu, and Yong Jae Lee. 2023. Visual instruction tuning. In *Advances in Neural Information Processing Systems*, pages 34892–34916.
- Wenzhuo Liu, Fei Zhu, Haiyang Guo, Longhui Wei, and Cheng-Lin Liu. 2025a. Llava-c: Continual improved visual instruction tuning. *arXiv preprint arXiv:2506.08666*.
- Yuyang Liu, Qiuhe Hong, Linlan Huang, Alexandra Gomez-Villa, Dipam Goswami, Xialei Liu, Joost van de Weijer, and Yonghong Tian. 2025b. Continual learning for vlms: A survey and taxonomy beyond forgetting. *arXiv preprint arXiv:2508.04227*.
- Pan Lu, Liang Qiu, Jiaqi Chen, Tony Xia, Yizhou Zhao, Wei Zhang, Zhou Yu, Xiaodan Liang, and Song-Chun Zhu. 2021. Iconqa: A new benchmark for abstract diagram understanding and visual language reasoning. *arXiv preprint arXiv:2110.13214*.
- Ahmed Masry, Xuan Long Do, Jia Qing Tan, Shafiq Joty, and Enamul Hoque. 2022. Chartqa: A benchmark for question answering about charts with visual and logical reasoning. In *Findings of the association for computational linguistics*, pages 2263–2279.
- Minesh Mathew, Viraj Bagal, Rubèn Tito, Dimosthenis Karatzas, Ernest Valveny, and CV Jawahar. 2022. Infographicvqa. In *Proceedings of the IEEE/CVF Winter Conference on Applications of Computer Vision*, pages 1697–1706.
- Minesh Mathew, Dimosthenis Karatzas, and CV Jawahar. 2021. Docvqa: A dataset for vqa on document images. In *Proceedings of the IEEE/CVF winter conference on applications of computer vision*, pages 2200–2209.
- Bryan A Plummer, Liwei Wang, Chris M Cervantes, Juan C Caicedo, Julia Hockenmaier, and Svetlana Lazebnik. 2015. Flickr30k entities: Collecting region-to-phrase correspondences for richer image-to-sentence models. In *Proceedings of the IEEE international conference on computer vision*, pages 2641–2649.
- Alec Radford, Jong Wook Kim, Chris Hallacy, Aditya Ramesh, Gabriel Goh, Sandhini Agarwal, Girish Sastry, Amanda Askell, Pamela Mishkin, Jack Clark, and 1 others. 2021. Learning transferable visual models from natural language supervision. In *International Conference on Machine Learning*, pages 8748–8763.
- Maryam Rahneemoonfar, Tashnim Chowdhury, Argho Sarkar, Debvrat Varshney, Masoud Yari, and Robin Roberson Murphy. 2021. Floodnet: A high resolution aerial imagery dataset for post flood scene understanding. *IEEE Access*, 9:89644–89654.
- María Virginia Sabando, Pavol Ulbrich, Matías Selzer, Jan Byška, Jan Mičan, Ignacio Ponzoni, Axel J Soto, María Luján Ganuza, and Barbora Kozlíková. 2020. Chemva: interactive visual analysis of chemical compound similarity in virtual screening. *IEEE Transactions on Visualization and Computer Graphics*, 27(2):891–901.
- Mingjie Sun, Zhuang Liu, Anna Bair, and Zico Kolter. 2024. A simple and effective pruning approach for large language models. In *International Conference on Learning Representations*, pages 4942–4964.
- Jun-Tao Tang, Yu-Cheng Shi, Zhen-Hao Xie, and Da-Wei Zhou. 2026. Prism: A plug-in reproducible infrastructure for scalable multimodal continual instruction tuning. *arXiv preprint arXiv:2605.26110*.
- Shengbang Tong, David Fan, Jiachen Li, Yunyang Xiong, Xinlei Chen, Koustuv Sinha, Michael Rabbat, Yann LeCun, Saining Xie, and Zhuang Liu. 2025. Metamorph: Multimodal understanding and generation via instruction tuning. In *Proceedings of the IEEE international conference on computer vision*, pages 17001–17012.
- Laurens Van der Maaten and Geoffrey Hinton. 2008. Visualizing data using t-sne. *Journal of machine learning research*, 9(11).
- Runyu Wang, Peng Ping, Zhengyu Guo, Xiaoye Zhang, Quan Shi, Liting Zhou, and Tianbo Ji. 2025a. Loki: Low-damage knowledge implanting of large language models. *arXiv preprint arXiv:2505.22120*.
- Xiao Wang, Tianze Chen, Qiming Ge, Han Xia, Rong Bao, Rui Zheng, Qi Zhang, Tao Gui, and Xuan-Jing Huang. 2023. Orthogonal subspace learning for language model continual learning. In *Findings of the Association for Computational Linguistics: EMNLP*, pages 10658–10671.
- Ziqi Wang, Chang Che, Qi Wang, Yangyang Li, Zenglin Shi, and Meng Wang. 2025b. Smolora: Exploring and defying dual catastrophic forgetting in continual visual instruction tuning. In *Proceedings of the IEEE international conference on computer vision*, pages 177–186.
- Zhen-Hao Xie, Jun-Tao Tang, Yu-Cheng Shi, Han-Jia Ye, De-Chuan Zhan, and Da-Wei Zhou. 2026. Same: Stabilized mixture-of-experts for multimodal continual instruction tuning. *arXiv preprint arXiv:2602.01990*.

- Shuo Yang, Caren Han, Siwen Luo, and Eduard Hovy. 2025. Magic-vqa: Multimodal and grounded inference with commonsense knowledge for visual question answering. In *Findings of the Proceedings of the Annual Meeting of the Association for Computational Linguistics: Proceedings of the Annual Meeting of the Association for Computational Linguistics*, pages 16967–16986.
- Yahan Yu, Duzhen Zhang, Yong Ren, Xuanle Zhao, Xiuyi Chen, and Chenhui Chu. 2025. Progressive lora for multimodal continual instruction tuning. In *Proceedings of the Annual Meeting of the Association for Computational Linguistics*, pages 2779–2796.
- Fanhu Zeng, Fei Zhu, Haiyang Guo, Xu-Yao Zhang, and Cheng-Lin Liu. 2025. Modalprompt: Towards efficient multimodal continual instruction tuning with dual-modality guided prompt. In *Proceedings of the Conference on Empirical Methods in Natural Language Processing*, pages 12137–12152.
- Shengyu Zhang, Linfeng Dong, Xiaoya Li, Sen Zhang, Xiaofei Sun, Shuhe Wang, Jiwei Li, Runyi Hu, Tianwei Zhang, Guoyin Wang, and 1 others. 2023a. Instruction tuning for large language models: A survey. *ACM Computing Surveys*.
- Xiaoman Zhang, Chaoyi Wu, Ziheng Zhao, Weixiong Lin, Ya Zhang, Yanfeng Wang, and Weidi Xie. 2023b. Pmc-vqa: Visual instruction tuning for medical visual question answering. *arXiv preprint arXiv:2305.10415*.
- Hengyuan Zhao, Ziqin Wang, Qixin Sun, Kaiyou Song, Yilin Li, Xiaolin Hu, Qingpei Guo, and Si Liu. 2025. Llava-cmoe: Towards continual mixture of experts for large vision-language models. *arXiv preprint arXiv:2503.21227*.
- Da-Wei Zhou, Qi-Wei Wang, Zhi-Hong Qi, Han-Jia Ye, De-Chuan Zhan, and Ziwei Liu. 2024. Class-incremental learning: A survey. *IEEE Transactions on Pattern Analysis and Machine Intelligence*, 46(12):9851–9873.
- Deyao Zhu, Jun Chen, Xiaoqian Shen, Xiang Li, and Mohamed Elhoseiny. 2023. Minigpt-4: Enhancing vision-language understanding with advanced large language models. *arXiv preprint arXiv:2304.10592*.
- Zhen Zhu, Yiming Gong, Yao Xiao, Yaoyao Liu, and Derek Hoiem. 2025. How to teach large multimodal models new skills. *arXiv preprint arXiv:2510.08564*.

A Theoretical Analysis of Geometry-aware Projection

In this section, we provide a theoretical justification for the geometry-aware decomposition in Eq. (16). We show that projecting the purified task update onto the group memory subspace extracts the optimal group-compatible component under the Frobenius norm, while the remaining residual captures task-specific directions that are orthogonal to the existing group memory.

A.1 Preliminaries

After task t is assigned to group g_t , we obtain its purified LoRA update

$$\Delta\hat{\Theta}_t = \mathbf{M}_t \odot \Delta\Theta_t, \quad (23)$$

where \mathbf{M}_t is the activation-aware binary mask. Let \mathcal{U}_{g_t} denote the subspace spanned by the current shared memory of group g_t . Intuitively, \mathcal{U}_{g_t} contains the parameter directions that have been consistently reused by previous tasks in the same group. Therefore, an update direction lying in \mathcal{U}_{g_t} can be viewed as group-compatible, while directions outside this subspace are more likely to encode task-specific deviations.

For notational simplicity, we consider the vectorized form of the update:

$$\mathbf{x}_t = \text{vec}(\Delta\hat{\Theta}_t) \in \mathbb{R}^d. \quad (24)$$

Let $\mathbf{U}_{g_t} \in \mathbb{R}^{d \times r}$ be an orthonormal basis of \mathcal{U}_{g_t} , where r is the dimension of the group subspace and

$$\mathbf{U}_{g_t}^\top \mathbf{U}_{g_t} = \mathbf{I}. \quad (25)$$

The orthogonal projection matrix onto \mathcal{U}_{g_t} is then

$$\mathbf{P}_{g_t} = \mathbf{U}_{g_t} \mathbf{U}_{g_t}^\top. \quad (26)$$

A.2 Optimality of the Projected Shared Update

We first show that the projected component is the closest group-compatible approximation to the purified task update.

Proposition 1. Given the purified task update $\Delta\hat{\Theta}_t$ and the group memory subspace \mathcal{U}_{g_t} , the projected update

$$\Delta\Theta_t^{\text{share}} = \text{proj}_{\mathcal{U}_{g_t}}(\Delta\hat{\Theta}_t) \quad (27)$$

is the optimal group-compatible approximation to $\Delta\hat{\Theta}_t$ under the Frobenius norm:

$$\Delta\Theta_t^{\text{share}} = \arg \min_{\mathbf{Z} \in \mathcal{U}_{g_t}} \left\| \Delta\hat{\Theta}_t - \mathbf{Z} \right\|_F^2. \quad (28)$$

Proof. Using the vectorized notation, problem (28) is equivalent to

$$\min_{\mathbf{z} \in \mathcal{U}_{g_t}} \|\mathbf{x}_t - \mathbf{z}\|_2^2. \quad (29)$$

Since $\mathbf{z} \in \mathcal{U}_{g_t}$, there exists a coefficient vector $\mathbf{a} \in \mathbb{R}^r$ such that

$$\mathbf{z} = \mathbf{U}_{g_t} \mathbf{a}. \quad (30)$$

Therefore, the optimization becomes

$$\min_{\mathbf{a}} \|\mathbf{x}_t - \mathbf{U}_{g_t} \mathbf{a}\|_2^2. \quad (31)$$

Taking the derivative of Eq. (31) with respect to \mathbf{a} and setting it to zero gives

$$-2\mathbf{U}_{g_t}^\top (\mathbf{x}_t - \mathbf{U}_{g_t} \mathbf{a}) = 0. \quad (32)$$

Thus,

$$\mathbf{U}_{g_t}^\top \mathbf{x}_t = \mathbf{U}_{g_t}^\top \mathbf{U}_{g_t} \mathbf{a}. \quad (33)$$

Because \mathbf{U}_{g_t} is orthonormal, we have

$$\mathbf{U}_{g_t}^\top \mathbf{U}_{g_t} = \mathbf{I}. \quad (34)$$

Therefore, the optimal coefficient is

$$\mathbf{a}^* = \mathbf{U}_{g_t}^\top \mathbf{x}_t. \quad (35)$$

Substituting \mathbf{a}^* back into $\mathbf{z} = \mathbf{U}_{g_t} \mathbf{a}$ yields

$$\mathbf{z}^* = \mathbf{U}_{g_t} \mathbf{U}_{g_t}^\top \mathbf{x}_t = \mathbf{P}_{g_t} \mathbf{x}_t. \quad (36)$$

Returning to the matrix form, this gives

$$\Delta\Theta_t^{\text{share}} = \text{proj}_{\mathcal{U}_{g_t}}(\Delta\hat{\Theta}_t). \quad (37)$$

Hence, the projection is the minimizer of Eq. (28). \square

This result shows that the projection is not an arbitrary decomposition. Among all updates that lie in the group memory subspace, it is the one that best reconstructs the current task update.

A.3 Orthogonality of the Task-specific Residual

After extracting the group-compatible component, the residual is defined as

$$\Delta\Theta_t^{\text{res}} = \Delta\hat{\Theta}_t - \Delta\Theta_t^{\text{share}}. \quad (38)$$

We next show that this residual is orthogonal to all directions in the group subspace.

Proposition 2. The residual component satisfies

$$\langle \Delta\Theta_t^{\text{res}}, \mathbf{Z} \rangle_F = 0, \quad \forall \mathbf{Z} \in \mathcal{U}_{g_t}. \quad (39)$$

Proof. In vectorized form, the residual is

$$\mathbf{x}_t^{\text{res}} = \mathbf{x}_t - \mathbf{P}_{g_t} \mathbf{x}_t = \mathbf{x}_t - \mathbf{U}_{g_t} \mathbf{U}_{g_t}^\top \mathbf{x}_t. \quad (40)$$

For any $\mathbf{z} \in \mathcal{U}_{g_t}$, there exists $\mathbf{b} \in \mathbb{R}^r$ such that

$$\mathbf{z} = \mathbf{U}_{g_t} \mathbf{b}. \quad (41)$$

Then,

$$\langle \mathbf{x}_t^{\text{res}}, \mathbf{z} \rangle = \left(\mathbf{x}_t - \mathbf{U}_{g_t} \mathbf{U}_{g_t}^\top \mathbf{x}_t \right)^\top \mathbf{U}_{g_t} \mathbf{b} \quad (42)$$

$$= \mathbf{x}_t^\top \mathbf{U}_{g_t} \mathbf{b} - \mathbf{x}_t^\top \mathbf{U}_{g_t} \mathbf{U}_{g_t}^\top \mathbf{U}_{g_t} \mathbf{b}. \quad (43)$$

Since $\mathbf{U}_{g_t}^\top \mathbf{U}_{g_t} = \mathbf{I}$, we have

$$\mathbf{U}_{g_t}^\top \mathbf{U}_{g_t} \mathbf{b} = \mathbf{b}. \quad (44)$$

Thus,

$$\langle \mathbf{x}_t^{\text{res}}, \mathbf{z} \rangle = \mathbf{x}_t^\top \mathbf{U}_{g_t} \mathbf{b} - \mathbf{x}_t^\top \mathbf{U}_{g_t} \mathbf{b} \quad (45)$$

$$= 0. \quad (46)$$

Therefore, the residual is orthogonal to the group memory subspace. Returning to the matrix form gives Eq. (39). \square

A.4 Interpretation for Continual Instruction Tuning

The above results provide a geometric explanation for the proposed consolidation strategy. The shared component

$$\Delta\Theta_t^{\text{share}} = \text{proj}_{\mathcal{U}_{g_t}}(\Delta\hat{\Theta}_t) \quad (47)$$

is the best approximation of the current task update within the group-compatible subspace. Therefore, absorbing this component into the group adapter introduces the part of the update that is most consistent with the historical memory of the assigned group.

Meanwhile, the residual

$$\Delta\Theta_t^{\text{res}} = \Delta\hat{\Theta}_t - \Delta\Theta_t^{\text{share}} \quad (48)$$

contains directions that cannot be represented by the current group memory. Because it is orthogonal to \mathcal{U}_{g_t} , directly merging it into the shared group adapter may introduce task-specific deviations into the group-level parameters. This is especially harmful in multimodal continual instruction tuning, where different tasks may share similar image-text semantics but require different response protocols.

Therefore, the projection-based decomposition naturally supports the design of PROTOADA:

Algorithm 1 ProtoAda Training (per task t)

Require: Task \mathcal{T}_t ; frozen backbone Θ_0 , encoders ($E_{\text{text}}, E_{\text{vis}}$); groups $\{\mathbf{p}_g, \mathbf{A}_g, \mathcal{U}_g\}$; global adapter $\mathbf{A}^{\text{shared}}$; residual bank

Ensure: Updated group adapters, residuals, and format predictor f_{fmt}

- 1: **Prototype construction:** Compute $\mathbf{p}_t^{\text{text}}, \mathbf{p}_t^{\text{vis}}$, and format code $\mathbf{c}_t^{\text{fmt}}$; fuse into task prototype \mathbf{q}_t (Eqs. (4)–(7)).
 - 2: **Format-aware assignment:** Compute similarities $s_{t,g}$ (Eq. (8)); assign to g_t or init new group via adaptive threshold (Eq. (9)); update prototype \mathbf{p}_{g_t} (Eq. (10)).
 - 3: **Adaptive growth:** Estimate layer sensitivity γ_ℓ via gradients (Eq. (12)); select top- M layers \mathcal{S}_t using γ_ℓ and group usage $u_{g_t,\ell}$ (Eq. (13)).
 - 4: **Task training:** Init LoRA on \mathcal{S}_t ; optimize with \mathcal{L}_{ce} to get update $\Delta\Theta_t$; train predictor $\hat{\mathbf{c}}_t^{\text{fmt}} = f_{\text{fmt}}(\mathbf{p}_t^{\text{text}})$ with MSE (Eq. (11)).
 - 5: **Geometry consolidation:** Purify $\Delta\Theta_t$ with activation norm to get $\Delta\hat{\Theta}_t$ (Eqs. (14)–(15)); project onto \mathcal{U}_{g_t} to decouple $\Delta\Theta_t^{\text{share}}$ and $\Delta\Theta_t^{\text{res}}$ (Eq. (16)).
 - 6: **Memory update:** Absorb $\Delta\Theta_t^{\text{share}}$ into \mathbf{A}_{g_t} with weight λ_{t,g_t} (Eq. (17)); compress $\Delta\Theta_t^{\text{res}}$ via SVD and store as \mathbf{R}_t (Eq. (18)).
 - 7: **Maintenance (every K tasks):** Promote dominant directions to $\mathbf{A}^{\text{shared}}$ (Eqs. (19)–(20)); prune redundant residuals based on coverage ratio ρ_t (Eq. (21)).
-

- the group-aligned component is consolidated into the shared group adapter for parameter reuse;
- the orthogonal component is stored separately as a compact residual to preserve task-specific behavior;
- the orthogonality between the two parts reduces interference between reusable knowledge and task-specific response conventions.

In this sense, the geometry-aware decomposition provides an optimal and interpretable mechanism for extracting group-compatible updates from task-specific LoRA increments.

B Algorithmic Description of PROTOADA

Algorithm 1 summarizes the per-task training procedure of PROTOADA in the continual instruction-tuning stream. For each incoming task, PROTOADA first constructs a format-aware prototype from visual semantics, language semantics, and response-format statistics, and uses it to assign the task to a compatible memory group or initialize a new group. After assignment, the method performs prototype-conditioned adaptive growth by combining layer-wise gradient sensitivity with the historical usage pattern of the assigned group, so that LoRA capacity is introduced only at layers that are important for the current task and reusable

Algorithm 2 ProtoAda Inference (Task-agnostic)

Require: Input (v, q) ; frozen backbone Θ_0 , encoders $(E_{\text{text}}, E_{\text{vis}})$; predictor f_{fmt} ; global adapter $\mathbf{A}^{\text{shared}}$; group adapters $\{\mathbf{A}_g\}$; residual bank $\{\mathbf{R}_r\}$

Ensure: Generated response y

- 1: **Input processing:** Compute descriptors \mathbf{p}^{text} and \mathbf{p}^{vis} via frozen encoders; predict format code $\hat{\mathbf{c}}^{\text{fmt}} = f_{\text{fmt}}(\mathbf{p}^{\text{text}})$ (Eq. (11)).
 - 2: **Query prototype construction:** Fuse visual, linguistic descriptors, and predicted $\hat{\mathbf{c}}^{\text{fmt}}$ to build the query prototype $\mathbf{q}_{\text{query}}$ (Eqs. (6)–(7)).
 - 3: **Memory retrieval:** Compute similarities s_g between $\mathbf{q}_{\text{query}}$ and group prototypes \mathbf{p}_g ; retrieve Top-K groups and calculate routing weights w_g (Eq. (22)).
 - 4: **Residual activation:** Compare $\mathbf{q}_{\text{query}}$ with stored residual prototypes \mathbf{q}_r to retrieve the subset of compatible task-specific residuals $\{\mathbf{R}_r\}$.
 - 5: **Response generation:** Augment Θ_0 with $\mathbf{A}^{\text{shared}}$, retrieved group adapters (scaled by w_g), and selected residuals $\{\mathbf{R}_r\}$; generate response y in a single forward pass.
-

within the group. The selected LoRA modules are then optimized with the task loss, while the format predictor is trained to infer the response-format code from input-side descriptors for task-agnostic inference. After training, the learned update is purified by activation-aware masking and decomposed according to the group memory geometry: the group-compatible component is absorbed into the group adapter, whereas the remaining task-specific component is compressed and stored as a residual. Periodic maintenance further promotes dominant reusable directions into the global shared adapter and prunes redundant residuals. This procedure enables PROTOADA to reuse compatible knowledge across tasks while preserving task-specific response conventions.

C Construction of Format Statistics

To incorporate response protocols into task grouping, we derive a task-level format code c_t^{fmt} from target responses. For each mini-batch, masked label positions are removed and only valid response tokens are used. The statistics are organized into four groups: mean of response length, variance of response length, token uncertainty, and template consistency. The mean of response length records the average normalized number of target tokens, which distinguishes short-answer, multiple-choice, and long-form generation protocols. The variance of response length measures the dispersion of response lengths across samples, reflecting whether the task follows a fixed output template or allows variable-length responses. Token uncertainty is measured by the normalized entropy of the empir-

Table 4: Task-order robustness of **PROTOADA** on UCIT. We report average accuracy (%) under three task sequences.

PROTOADA (Ours)	Original	Reverse	Random
Avg. Accuracy (%)	74.66	70.83	71.17

ical token distribution and the unique-token ratio, characterizing how diverse or constrained the target responses are. Template consistency is estimated from the repetition ratio and coarse token-id distribution statistics, including the normalized token-id mean and standard deviation as well as low- and middle-band token-id ratios, which serve as tokenizer-independent proxies for option markers, numbers, punctuation, and repeated answer patterns. We average these batch-level statistics over the warm-up batches to obtain a fixed-dimensional task-level descriptor $\mathbf{c}_t^{\text{fmt}}$, which is then used for format-aware prototype construction.

D Robustness of Task Order

To evaluate whether PROTOADA depends on a favorable task curriculum, we further examine its robustness to task ordering on the UCIT benchmark. Specifically, we report the average accuracy under three different task sequences:

- **Original:** the canonical task order defined by the benchmark protocol;
- **Reverse:** the exact reverse of the original sequence, where the last task is presented first;
- **Random:** a randomly shuffled task order. For reproducibility, we fix the random permutation as:

UCIT: Flickr30k \rightarrow CLEVR \rightarrow ArxivQA \rightarrow ImageNet-R \rightarrow IconQA \rightarrow VizCap.

As shown in Tab. 4, PROTOADA maintains stable performance under different task orders, achieving 74.66%, 70.83%, and 71.17% average accuracy under the Original, Reverse, and Random sequences, respectively. Although reversing or shuffling the task order introduces a moderate performance drop, PROTOADA still preserves competitive accuracy without relying on the canonical curriculum. This robustness mainly benefits from three designs. First, *format-aware task grouping* assigns each incoming task according to a prototype that jointly captures visual semantics, language semantics, and response-format statistics, thereby

reducing the chance of merging tasks with incompatible instruction protocols. Second, *prototype-conditioned adaptive growth* introduces LoRA capacity only in layers that are sensitive to the current task and historically useful for the assigned group, which mitigates unnecessary perturbation to previously learned behaviors. Third, *geometry-aware consolidation* separates group-compatible update directions from task-specific residuals, allowing reusable knowledge to be absorbed into group memory while preserving task-specific deviations separately. Together, these mechanisms reduce order-dependent interference and make PROTOADA more suitable for continual multimodal instruction tuning under non-stationary task arrivals.

E Brief Description of Compared Methods

Zero-shot. This baseline directly evaluates the frozen pre-trained LLaVA model on the complete task sequence without updating any parameters. It reflects the intrinsic cross-task generalization ability of the original multimodal backbone.

FT-LoRA. FT-LoRA performs continual instruction tuning with standard LoRA adapters. For each incoming task, the model is trained sequentially by updating only the LoRA parameters, while the pre-trained backbone remains fixed. No explicit mechanism is introduced to mitigate forgetting across tasks.

Replay-LoRA. Replay-LoRA extends sequential LoRA fine-tuning with an episodic memory buffer. A small number of samples from previous tasks are stored and mixed with the current task data during training, so that the model can rehearse earlier knowledge while adapting to new instructions.

MoE-LoRA (Chen et al., 2024). MoE-LoRA equips the backbone with multiple LoRA experts and learns a routing function to combine their outputs. Instead of relying on a single adapter, the model dynamically aggregates expert-specific adaptations, providing additional capacity for heterogeneous tasks in continual tuning.

HiDe-LLaVA (Guo et al., 2025a). HiDe-LLaVA adopts a task-aware expert decomposition strategy for multimodal continual instruction tuning. It maintains task-associated LoRA experts and activates the corresponding expert during training. At test time, the task identity is estimated by matching CLIP-based visual and textual anchors, which are then used to select the most relevant expert.

CL-MoE (Huai et al., 2025). CL-MoE introduces an input-dependent mixture-of-experts mechanism for continual multimodal instruction tuning. It performs fine-grained routing at the layer and token levels, allowing different tokens to access different experts without requiring explicit task identifiers. Combined with memory replay, it serves as a strong task-agnostic continual learning baseline.

DISCO (Guo et al., 2025b). DISCO builds task prototypes from CLIP image and text representations and uses them to guide expert aggregation. During inference, the similarity between the current input and stored task prototypes determines diagonal mask weights over LoRA experts, enabling prototype-based routing in the absence of explicit task IDs.

ModalPrompt (Zeng et al., 2025). ModalPrompt is a prompt-based continual learning method that assigns learnable soft prompts to different tasks. In inference, the model retrieves the most relevant prompts according to dual-modal guidance from image and text features. A balancing coefficient controls the relative contribution of visual and textual cues during prompt selection.

SAME (Xie et al., 2026). SAME exploits spectral information from LoRA parameter updates to identify stable task-related directions. It incrementally performs singular value decomposition over recent LoRA statistics and retains dominant spectral anchors for knowledge consolidation. A curvature-aware importance measure is further used to regulate parameter updates and reduce interference among tasks.